Received: 17 March 2020 | Revised: 5 June 2020 | Accepted: 12 July 2020

DOI: 10.1002/bit.27495

ARTICLE

BIOTECHNOLOGY BIOENGINEERING WILEY

Characterization of glutathione proteome in CHO cells and its relationship with productivity and cholesterol synthesis

Valentine Chevallier[1,2] | Erwin M. Schoof[2] | Laetitia Malphettes[3] | Mikael R. Andersen[2] | Christopher T. Workman[2]

[1]Upstream Process Sciences, UCB Nordic A/S, Copenhagen, Denmark

[2]Department of Biotechnology and Biomedicine, Technical University of Denmark, Lyngby, Denmark

[3]Upstream Process Sciences, UCB Pharma SA, Braine l'Alleud, Belgium

Correspondence
Christopher T. Workman, Department of Biotechnology and Biomedicine, Technical University of Denmark, Søltoft Plads, Building 223, 2800 Lyngby, Denmark.
Email: cwor@dtu.dk

Funding information
Innovationsfonden, Grant/Award Number: 5189-00037B; UCB Nordic A/S

Abstract

Glutathione (GSH) plays a central role in the redox balance maintenance in mammalian cells. Previous studies of industrial Chinese hamster ovary cell lines have demonstrated a relationship between GSH metabolism and clone productivity. However, a thorough investigation is required to understand this relationship and potentially highlight new targets for cell engineering. In this study, we have modulated the GSH intracellular content of an industrial cell line under bioprocess conditions to further elucidate the role of the GSH synthesis pathway. Two strategies were used: the variation of cystine supply and the direct inhibition of the GSH synthesis using buthionine sulfoximine (BSO). Over time of the bioprocess, a correlation between intracellular GSH and product titer has been observed. Analysis of metabolites uptake/secretion rates and proteome comparison between BSO-treated cells and nontreated cells has highlighted a slowdown of the tricarboxylic acid cycle leading to a secretion of lactate and alanine in the extracellular environment. Moreover, an adaptation of the GSH-related proteome has been observed with an upregulation of the regulatory subunit of glutamate–cysteine ligase and a downregulation of a specific GSH transferase subgroup, the Mu family. Surprisingly, the main impact of BSO treatment was observed on a global downregulation of the cholesterol synthesis pathways. As cholesterol is required for protein secretion, it could be the missing piece of the puzzle to finally elucidate the link between GSH synthesis and productivity.

KEYWORDS

buthionine sulfoximine, CHO cells, cholesterol, glutathione, proteomics

1 | INTRODUCTION

Under bioprocess conditions, Chinese hamster ovary (CHO) cells can be exposed to oxygen microheterogeneity, free radicals generated by cell culture medium components and high oxidative metabolism, which can lead to oxidative stress. Moreover, product quality can also be affected by reactive oxygen species (ROS) production. For these and other reasons, research related to the control of oxidative stress has been of increased interest. In this context, the controlled modulation of oxidative stress can help scientists to improve bioprocesses.

One of the main targets for the modulation of oxidative stress is glutathione (GSH). GSH is a tripeptide (γ-L-glutamyl-L-cysteinyl glycine)

which is the cofactor of ROS detoxification enzymes, as well as a direct ROS scavenger. GSH can also form conjugates with reactive electrophilic compounds to promote their detoxification (Ketterer, Coles, & Meyer, 1983). It plays a central role in the detoxification of ROS produced in the mitochondria, but also in the regulation of disulfide bond formation in the endoplasmic reticulum (Chakravarthi & Bulleid, 2004; Ribas, García-Ruiz, & Fernández-Checa, 2014).

A potential relationship between GSH and secreted protein productivity has already been suggested in literature. High-producing cell lines have been shown to contain more GSH than low producers and an upregulated GSH metabolism (Chong et al., 2012; Orellana et al., 2015). To reproduce this phenomenon, cell engineering has been performed to increase GSH synthesis (Orellana, Marcellin, Gray, & Nielsen, 2017). On one hand, overexpression of the catalytic subunit of glutamate–cysteine ligase (GCLc), the rate-limiting enzyme in GSH synthesis, did not lead to increased titers despite higher GSH levels. On the other hand, the overexpression of the regulatory subunit of GCLc also called the glutamate–cysteine ligase modifier (GCLm) subunit led to an increase of productivity.

The uncertainty around the actual role of GSH in CHO bioprocessing led us to investigate the role of this metabolite further. Indeed, if the absolute GSH quantity does not explain productivity between two different clones, can it explain productivity differences between two processes with the same clone? What are the other cellular functions that are directly or indirectly impacted by the intracellular levels of GSH? In this context, we have modulated intracellular GSH levels using two approaches: the variation of cystine supply through feed medium composition and direct inhibition of the GCL enzyme using buthionine sulfoximine (BSO). Our goal was to understand which pathways are actually affected by lower levels of GSH. To capture the metabolic adaptations to these two variations, we investigated the cell phenotype, measured metabolites involved in the central carbon metabolism, and performed proteomic analysis.

2 | MATERIALS AND METHODS

2.1 | Cell culture

A proprietary DG44 CHO cell line engineered to produce a full monoclonal antibody was used. These cells were cultivated for 14 days in 2-L glass bioreactors (Sartorius) with dissolved oxygen and pH control. Bioreactors were inoculated on Day 0 at a seeding density of 0.35×10^6 cells/ml. Cells were cultivated in fed-batch mode with addition of feeds from Day 3 to Day 12. Viable cell concentration (VCC) and viability were measured using a Vi-Cell analyzer (Beckman Coulter). Recombinant protein titer was measured by immunoturbidimetry using a Cedex Bio HT analyzer (Roche) in the supernatant.

Two processes have been assessed to produce this recombinant protein: Process 1 and Process 2. In the upstream part, Process 2 has a less concentrated feed medium, especially with less cysteine. To mimic oxidative stress during the culture, L-buthionine sulfoximine (BSO; Sigma-Aldrich) was spiked on Day 3 to a final concentration of 0.5 mM in the bioreactor. This concentration has been selected based on previous screening experiment performed in shake flasks. BSO concentration below 0.5 mM did not lead to differences in VCC and monoclonal antibody (mAb) specific productivity despite lower GSH content (Figures S1–S3). To ensure the capture of metabolic changes related to GSH, 0.5-mM BSO treatment has been used in this study. All conditions have been performed in triplicates. One bioreactor cultivated with Process 2 and without BSO has been excluded from the dataset due to pump failure during the culture.

2.2 | Amino acid measurement

The cell culture fluid was centrifuged for 30 min at 17,000*g* in a 3K Amicon® 0.5-ml Filter (Merck). The sample preparation and analysis were performed by reverse-phase ultraperformance liquid chromatography as described previously (Mulukutla et al., 2019) using a TUV detector (Waters) set at 254 nm.

2.3 | GSH measurement

After sampling, the cell culture fluid was directly quenched using a −20°C ethanol bath and kept cold in a CoolRack® (Corning) during the sample preparation. A volume containing 10^7 cells was then centrifuged at 1,000*g*, 1 min, −5°C. Cell pellets were washed twice using cold 0.9% NaCl solution and frozen at −80°C. The day of the analysis, the cell pellet was resuspended in a 10 mM ethylenediaminetetraacetic acid solution (pH 8) and a ^{13}C-labeled GSH internal standard (Buchem) was added. Cells were lysed using a sonifier (Brandson) for 30 s (pulse mode [15 s on/5 s off]) with a 10% amplitude. To measure total GSH, a dithiothreitol solution was added to the lysate and incubated for 30 min at room temperature to reduce GSH disulfide. After 30 min, *N*-ethylmaleimide stock solution was added and incubated for 40 min at room temperature, protected from light. Proteins were then precipitated by the addition of −20°C acetone. After precipitation, the samples were centrifuged at 17,000*g* for 5 min and the supernatant was transferred to a new tube for overnight evaporation (CentriVap® Centrifugal Concentrators, Labconco). The sample pellet was reconstituted in mobile phase A (0.1% formic acid:water) using sonication. The sample was analyzed by liquid chromatography–mass spectrometry (MS) using a tandem quadrupole detector (Waters). The liquid chromatography was performed on an HSST 3 column of 10 cm (Waters) at 45°C and under a gradient of mobile phases A and B (0.1% formic acid:acetonitrile). GSH quantity were determined by comparison with the internal standard and normalized by the cell quantity.

2.4 | Sample preparation for proteomics analysis

Cells (5×10^7) were harvested on Days 6 and 10 of the culture, quenched using a −20°C ethanol bath and kept cold in a CoolRack®

(Corning) during the sample preparation. Cells were spun down at 1,000*g*, 1 min, −5°C. The cell pellets were washed two times with cold 0.9% NaCl solution. Proteins were extracted in 1 ml of 6 M guanidine solution, boiled for 5 min at 95°C, and vortexed. Samples were then spun down for 10 min at 17,000*g* and supernatants were stored at −80°C. Protein concentration was determined in samples diluted 10 times following the protocol of the Pierce™ BCA Protein assay (Thermo Fisher Scientific). An internal standard has been generated by pooling equal proteins amount of all the samples analyzed. Fifty micrograms of each samples was reduced and alkylated using Tris(2-carboxyethyl)phosphine and chloroacetamide at a final concentration of 10 and 40 mM, respectively. Samples were diluted 1:3 with 10% acetonitrile, 50 mM HEPES pH 8.5, LysC (MS grade; Wako) was added in a 1:50 (enzyme to protein) ratio, and samples were incubated at 37°C for 4 hr. Samples were further diluted to 1:10 with 10% acetonitrile, 50 mM HEPES pH 8.5, trypsin (MS grade; Promega) was added in a 1:100 (enzyme to protein) ratio and samples were incubated overnight at 37°C. Enzyme activity was quenched by adding 2% trifluoroacetic acid (TFA) to a final concentration of 1%. Before TMT labeling, the peptides were desalted on in-house packed C18 Stagetips (Rappsilber, Mann, & Ishihama, 2007). For each sample, two disks of C18 material (3M Empore) were packed in a 200-µl tip, and the C18 material activated with 40 µl of 100% methanol (HPLC grade; Sigma-Aldrich), then 40 µl of 80% acetonitrile, 0.1% formic acid. The tips were subsequently equilibrated 2× with 40 µl of 1% TFA, 3% acetonitrile, after which 10 µg of the sample was loaded using centrifugation at 4,000 rpm. After washing the tips twice with 100 µl of 0.1% formic acid, the peptides were eluted into clean 500-µl Eppendorf tubes using 40% acetonitrile, 0.1% formic acid. The eluted peptides were concentrated in an Eppendorf Speedvac, and reconstituted in 50-mM HEPES (pH 8.5) for TMT labeling. Labeling was done according to the manufacturer's instructions, and subsequently, labeled peptides were mixed in equimolar amounts (11-plex), acidified to 1% TFA and acetonitrile concentration brought down to <5% using 2% TFA. Processes 1 and 2 samples have been split between four different TMT 11-plexed samples. Biological replicates were intentionally distributed in different TMT 11-plexed samples (different labeling reactions). Three samples were run in triplicate (technical replicates) to assess the variability between TMT labeling reactions.

Before MS analysis, the peptides were fractionated using an offline Thermo Fisher Scientific Ultimate 3000 liquid chromatography system using high pH fractionation (5 mM ammonium bicarbonate, pH 10) at 5 µl/min flowrate. Thirty micrograms of peptides were separated over a 120-min gradient (5–35% acetonitrile), while collecting fractions every 120 s. The resulting 60 fractions were pooled into 28 final fractions, acidified to pH < 2 with 1% TFA and loaded onto EvoSep stagetips according to manufacturer's protocol.

2.5 | MS data acquisition

For each fraction, peptides were analyzed using the preset "30 samples per day" method on the EvoSep One instrument. Peptides were eluted over a 44-min gradient, and analyzed on a Q-Exactive HF-X instrument (Thermo Fisher Scientific) running in a DD-MS2 top 20 methods. Full MS spectra were collected at a resolution of 120,000, with an AGC target of 3×10^6 or maximum injection time of 50 ms and a scan range of 350–1,500 m/z. The MS2 spectra were obtained at a resolution of 45,000, with an AGC target value of 1×10^5 or maximum injection time of 96 ms, normalized collision energy of 32, and an intensity threshold of 1.e5. First mass was set to 110 m/z to ensure capture of the TMT reporter ions. Dynamic exclusion was set to 20 s, and ions with a charge state <2, >6 and unknown were excluded. MS performance was verified for consistency by running complex cell lysate quality control standards, and chromatography was monitored to check for reproducibility.

2.6 | Proteomics data analysis

MS spectra were processed using the TMT reporter ion quantitation from Proteome Discoverer (Thermo Fisher Scientific, version 2.2) and the MS Amanda identification algorithm (Dorfer et al., 2014). The MS/MS data were queried against the CHO-K1 proteome available from UniProtKB (proteome ID: UP000001075, downloaded September 3, 2018) and the "common Repository of Adventitious Proteins" database for contaminants available on the Global Proteome Machine website (downloaded October 30, 2018; Craig, Cortens, & Beavis, 2004; UniProt Consortium, 2018). Precursor mass tolerance was set at 10 ppm. Fragment mass tolerance was set at 0.02 ppm. Methionine oxidation and protein N-terminal acetylation were defined as dynamic modifications. Cysteine carbamidomethylation, TMT adduction on lysine and on protein N-terminal were defined as a fixed modification. Peptides and assembled proteins were searched at a false discovery rate (FDR) of 1%. The identified protein set has been filtered depending on multiple the identification confidence criteria: a high FDR confidence provided by PD software that is based on the comparison with decoy proteins and the MS Amanda scoring and a minimum of one unique peptide. Moreover, proteins not detected in the internal standard of each TMT samples have been removed from the dataset. For TMT quantification, the ratios of the TMT reporter ion intensities between samples and the internal standard (label 131C), generated by Proteome Discoverer for each protein, were used. These ratios were extracted for the statistical analysis in R.

2.7 | Statistical analysis

Ratios extracted from Proteome discoverer were log2 transformed and quantiles normalized in R. These data were then used to perform an empirical Bayes moderated *t* test using the *limma* package in R (Phipson, Lee, Majewski, Alexander, & Smyth, 2016; Ritchie et al., 2015). Effect of the parameter day, BSO treatment, and process have been included in the design matrix. Differentially expressed proteins were identified using an adj. $p < .05$. To narrow down the analysis, we focused only on proteins differentially expressed

because of the BSO treatment and with a log fold change (logFC) threshold of 0.5. A heatmap of the differentially expressed proteins was generated by hierarchical clustering using *pheatmap* package in R (Kolde, 2015). Functional analyses were performed using MetaCore (version 19.2.69700; Clarivate Analytics) after protein ID conversion to the *Mus musculus* equivalents. The ID conversion was performed using InParanoid 8 and UniProtKB BLAST when no matches were found in the first method (Sonnhammer & Ostlund, 2015).

3 | RESULTS

3.1 | Delayed impact of BSO on growth

To study the effect of GSH on recombinant mAb production, GSH was depleted using BSO. A sterile BSO solution was spiked on Day 3 of the fed batch culture to a final BSO concentration of 0.5 mM. BSO-treated bioreactors and control bioreactors were monitored by daily measurement of VCC, intracellular GSH, and product titer. Surprisingly, despite a depletion of GSH already observed on Day 4, that is, 24 hr after BSO addition, the growth and production profiles only started to differ from Day 6 (Figure 1). The average cell diameter started to increase from Day 6 in the BSO condition instead of Day 8 in control condition (Figure S4). Furthermore, the decrease in viability was only observed from Day 9 in BSO conditions despite a treatment on Day 3 (Figure S4). These results suggest that the CHO cell line phenotype was unaffected by GSH depletion during the three first days after BSO addition. From Day 6, their growth rate was gradually reduced, and their cellular volume is increasing until Day 10. The viable cell concentration decreased after Day 10 due to cell death until the end of the culture.

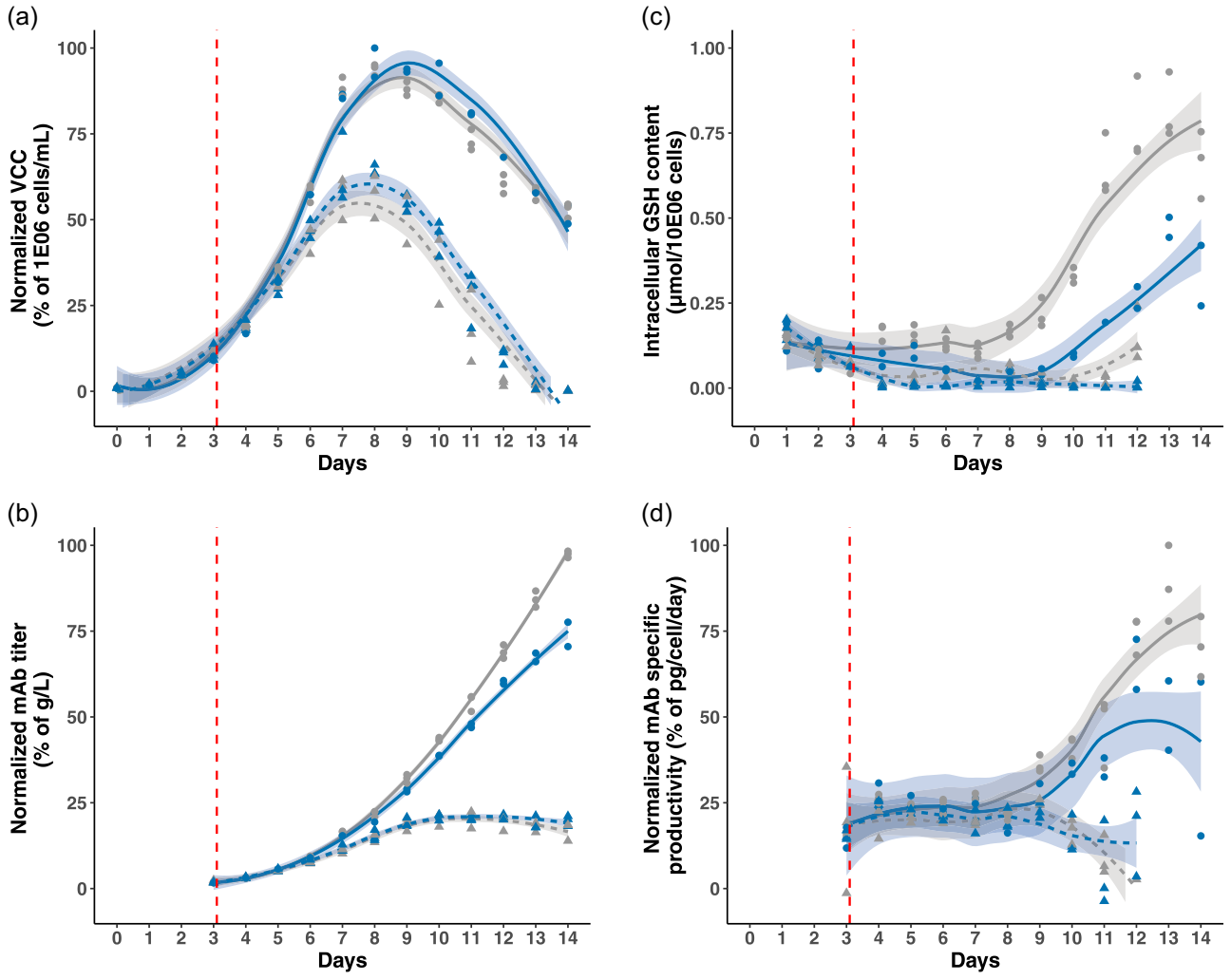

FIGURE 1 Effect of BSO treatment on cell growth, productivity, and GSH content. Gray and blue indicates the feed medium used—control feed medium or low cysteine feed medium, respectively. Circles indicate nontreated bioreactors and triangles indicate BSO-treated bioreactors. The red dotted lines represent the timing of BSO addition to a medium concentration of 0.5 mM. (a) viable cell concentration (VCC) profile. (b) Product titer in the supernatant over time. (c) Intracellular GSH concentration overtime. (d) mAb specific productivity over time. BSO, buthionine sulfoximine; GSH, glutathione; mAb, monoclonal antibody [Color figure can be viewed at wileyonlinelibrary.com]

3.2 | Cysteine supply modulates intracellular GSH and product titer

Since cysteine is a precursor of GSH, we also investigated if this lower concentration of cysteine influenced the content of intracellular GSH during the cultivation using a feed (Process 2) containing lower levels of cysteine (Figure 1c). A correlation between the increase of total GSH and the increase in specific productivity was observed over time.

Except for product titer, no other significant differences between the two feeding strategies were observed in growth profile, proteomic data, and metabolites uptake and production rate. As a result, data from the two feeding strategies (Processes 1 and 2) were combined to study the BSO effect in the next analysis.

3.3 | BSO treatment affects metabolite secretion and uptake rates

To further characterize the impact of GSH depletion on CHO cell line metabolism, daily extracellular concentrations of selected metabolites were measured and associated specific uptake and production rate were calculated. Uptake/secretion rates of glucose, lactate, and amino acids are shown in Figures 2 and S5. Glucose uptake rates were similar between control and BSO conditions until Day 10. Glucose uptake was slightly faster in the BSO condition compared to the control when viability and cell diameter started to decrease. Similar profiles were also observed for histidine, asparagine, and tyrosine uptake rate from Day 10. On the contrary, hydroxyproline and aspartic acid were produced/released from this point. These metabolic changes seem to be more related to cell death than to the BSO stress itself. The production

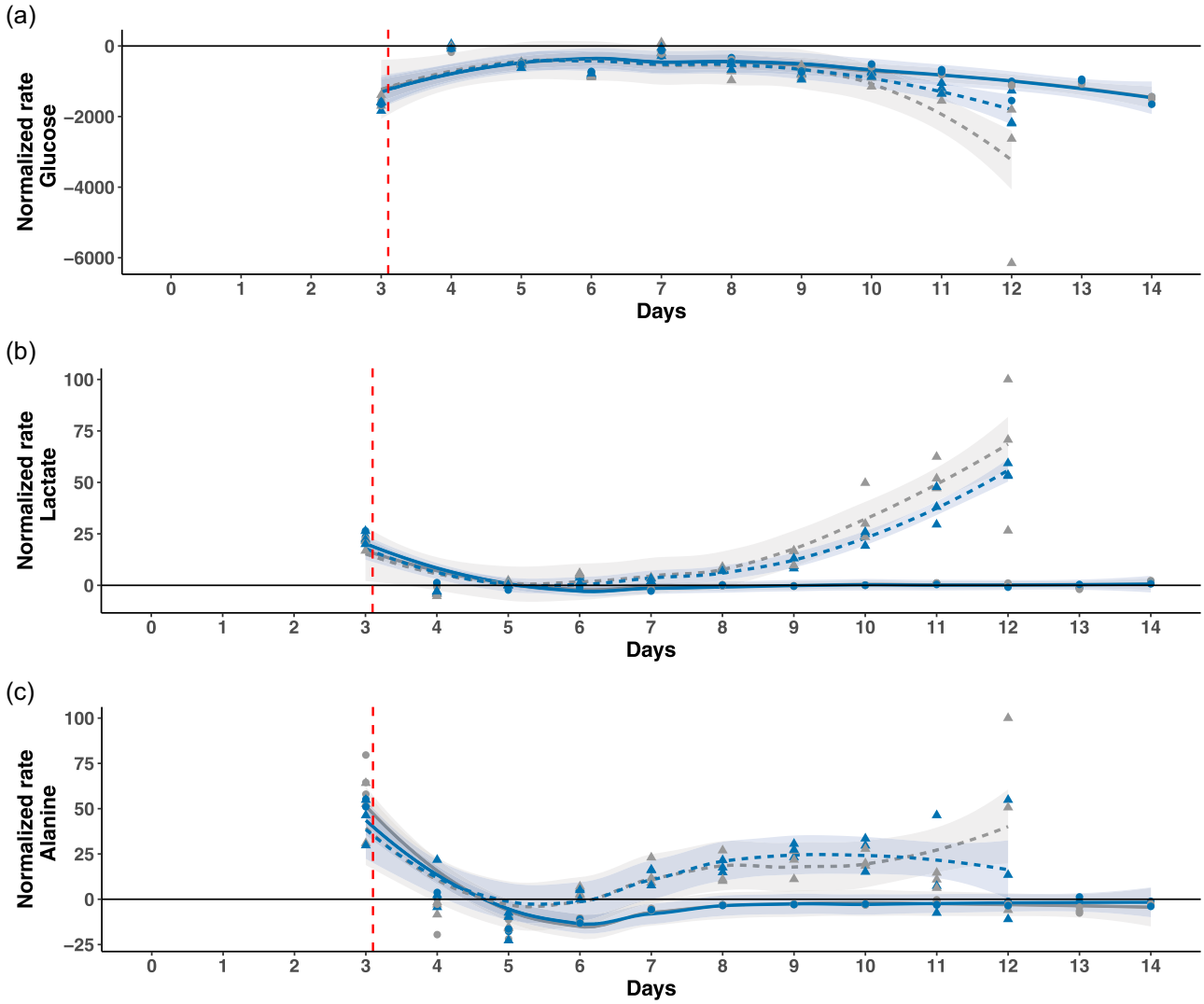

FIGURE 2 Effect of BSO treatment on glucose, lactate, and alanine uptake/secretion rates. Gray and blue indicates the feed medium used—control feed medium or low cysteine feed medium, respectively. Circles indicate nontreated bioreactors and triangles indicate BSO-treated bioreactors. The red dotted lines represent the timing of BSO addition to a medium concentration of 0.5 mM. (a) Glucose rate. (b) Lactate rate. (c) Alanine rate. BSO, buthionine sulfoximine [Color figure can be viewed at wileyonlinelibrary.com]

of cystine observed from Day 8 suggests a cysteine secretion, but high variability was observed for this amino acid in the BSO conditions.

Lactate uptake/secretion rate already started to differ from Day 6. Indeed, lactate is produced by BSO-treated cells and consumed by nontreated cells. Regarding amino acid uptake/secretion rates, alanine was the only amino acid that displayed a similar profile to lactate in response to the BSO treatment. Since lactate and alanine can be produced from pyruvate, these profiles suggest failure or slowdown of the tricarboxylic acid (TCA) cycle.

3.4 | Proteome related to TCA cycle, GSH metabolism, and cholesterol biosynthesis are modulated by BSO treatment

As GSH metabolism is seemingly linked to the clone productivity, we evaluated the impact of GSH depletion on cellular proteins expression in the studied cell line. For this purpose, we sampled 50×10^6 cells on Days 6 and 10 to perform proteomics analysis using TMT labeling (see Section 2). Across all samples, 3,281 proteins were identified with the identification criteria defined in Section 2.

Differentially expressed proteins in the BSO-treated culture have been identified using an empirical Bayes moderated *t* test (adj. $p < .05$, LogFC threshold: 0.5). This analysis was done on data from Day 6 and Day 10, that is, 3 and 7 days after treatment (Table S1). In total, 63 proteins were differentially expressed in response to BSO; 47 proteins were downregulated, and 16 proteins were upregulated. A heatmap of the differentially expressed proteins is shown in Figure 3. No pattern can be observed between data from Process 1 versus Process 2. The global protein expression was not impacted by a low cysteine supply in contrast to the product titer and intracellular GSH content. Overall, except for a few proteins, the BSO impact on proteins levels observed on Day 6 was amplified on Day 10.

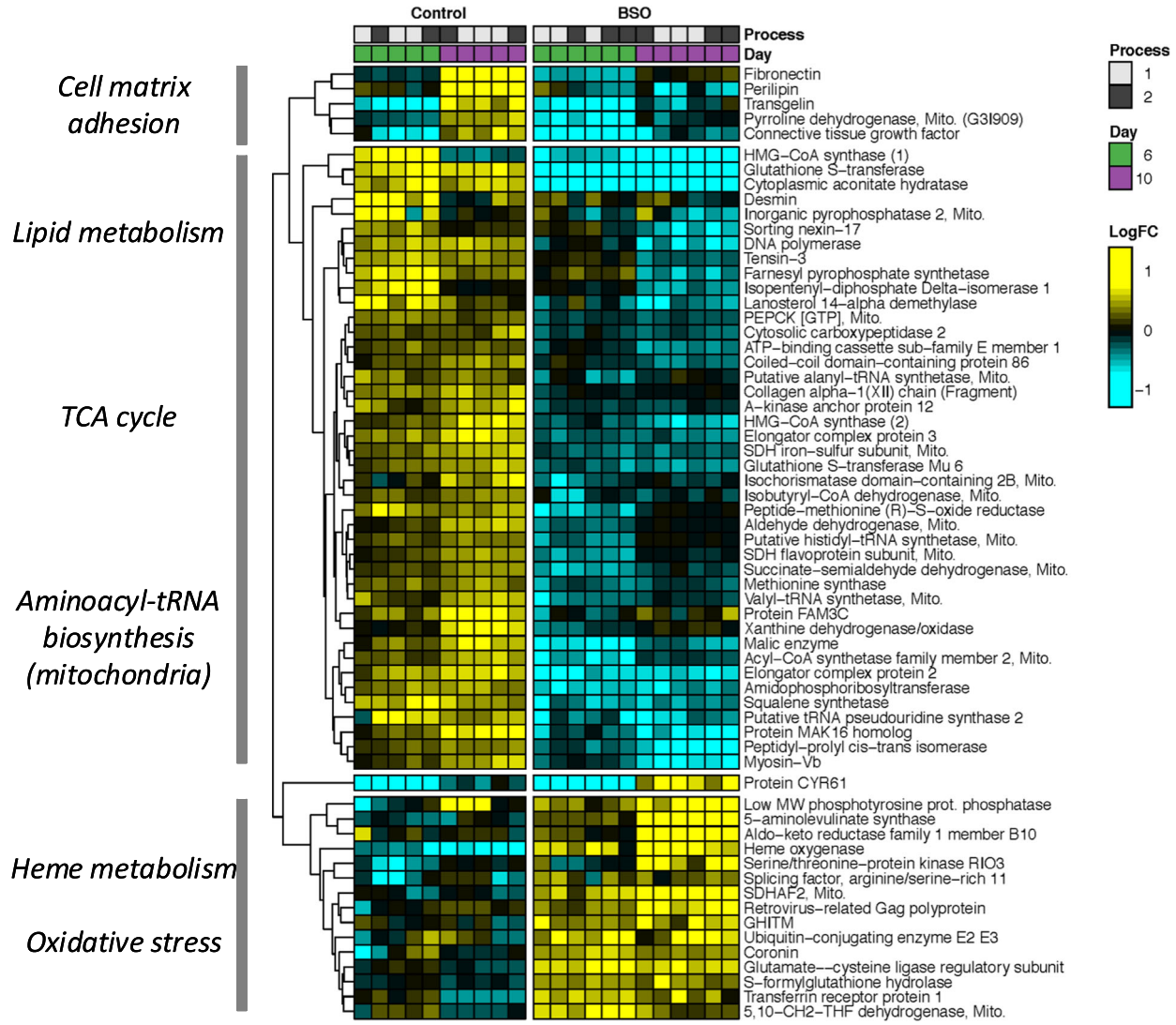

FIGURE 3 Heatmap of differentially expressed proteins under BSO treatment in CHO cells. Main cellular function of proteins cluster has been added in the figure. BSO, buthionine sulfoximine; CHO, Chinese hamster ovary; HMG-CoA, 3-hydroxy-3-methylglutaryl coenzyme A; TCA, tricarboxylic acid [Color figure can be viewed at wileyonlinelibrary.com]

To identify the cellular functions most impacted by the BSO treatment, enrichment analysis on differentially expressed proteins was performed in Metacore software based on GO annotations and Pathway maps (Table S2). Based on these results, each cluster identified on the heatmap has been associated with overrepresented functions (Figure 3). In the first cluster, protein expression increased significantly between Day 6 and Day 10 for the control condition, while proteins expression remained low at Day 10 for the BSO condition. This cluster primarily represented cell-matrix adhesion proteins. This observation can be associated to cell growth differences observed on Day 10 between the two conditions. Likewise, the opposite response observed for CYR61 protein can also be linked to cell growth response as this protein is a known regulator of apoptosis (Lau, 2011).

The largest cluster of proteins were downregulated after BSO treatment on both Days 6 and 10 (Figure 3; Table 1). These included three main functions: cholesterol biosynthesis, carboxylic acid metabolism, and aminoacyl-t-RNA biosynthesis in mitochondria. These cellular processes were interpreted to be at least partially downregulated in the BSO conditions relative to the control. All detected enzymes involved in cholesterol biosynthesis were downregulated with an average logFC between −0.34 and −1.21 (Table 1). Interestingly the related transcription factor SREBP2 was also downregulated but to a lesser extent (logFC: −0.17/adj. $p < .05$).

When we specifically considered mitochondrial proteins related to the TCA cycle, a global downregulation was observed where 12 mitochondrial proteins were observed to have logFC in the interval [−1.09, −0.13] and adj. $p < .05$ (Table 1). However, glycolysis-related proteins were not differentially expressed (Table S1).

In the last cluster (Figure 3), the main response to oxidative stress was observed, as this contains the majority of BSO upregulated proteins, including three proteins were related to heme metabolism. Heme oxygenase had the strongest signal with a logFC of 1.50 and has also been associated with oxidative stress (Hedblom et al., 2019).

Proteins specifically involved in GSH metabolism can be found in the two last described clusters (Figure 3). More details about proteins detected related to GSH are presented in Figure 4. GSH synthesis-related proteins were overall upregulated, especially the glutamate–cysteine ligase regulatory subunit and the S-formylGSH hydrolase. In contrast, some proteins involved in the consumption of GSH, for example, for the detoxification or catabolism of GSH, were overall downregulated. A good example of this was the downregulation of GSH S-transferases from the Mu family. However, GSTs

TABLE 1 Cholesterol and TCA cycle-related proteins expression in BSO-treated cells

Pathway	Uniprot accession	Protein names	LogFC	Adj. *p*
TCA cycle	G3H5K6	Pyruvate dehydrogenase E1 component subunit alpha	−0.46	2.43×10^{-7}
	G3HRP3	Citrate synthase	0.12	5.09×10^{-3}
	G3II47	Aconitate hydratase, mitochondrial (Aconitase; EC 4.2.1.-)	−0.20	6.38×10^{-5}
	G3H450	Isocitrate dehydrogenase (NAD) subunit, mitochondrial	−0.19	2.07×10^{-3}
	G3H0B5	Isocitrate dehydrogenase (NAD) subunit, mitochondrial	−0.10	1.70×10^{-2}
	G3HSW9	Isocitrate dehydrogenase (NAD) subunit, mitochondrial	−0.13	2.46×10^{-2}
	G3HU51	Isocitrate dehydrogenase (NADP)	−0.34	2.84×10^{-7}
	G3IHC0	Isocitrate dehydrogenase (NADP)	−0.13	2.87×10^{-3}
	G3HMB4	2-Oxoglutarate dehydrogenase E1 component, mitochondrial	0.02	6.09×10^{-1}
	G3IP00	Succinyl-CoA ligase (ADP-forming) subunit beta, mitochondrial	0.10	3.13×10^{-1}
	G3HZ50	Succinyl-CoA ligase (ADP-forming) subunit beta, mitochondrial	0.04	5.68×10^{-1}
	G3HQ05	Succinate-CoA ligase (ADP/GDP-forming) subunit alpha, mitochondrial	−0.01	8.58×10^{-1}
	G3GS40	Succinyl-CoA ligase (GDP-forming) subunit beta, mitochondrial	−0.26	9.59×10^{-7}
	G3IFX1	Succinate dehydrogenase (ubiquinone) flavoprotein subunit, mitochondrial	−0.60	7.66×10^{-12}
	G3IEY0	Succinate dehydrogenase (ubiquinone) iron-sulfur subunit, mitochondrial	−0.73	1.65×10^{-11}
	G3H6M5	Fumarate hydratase, mitochondrial	0.06	1.56×10^{-1}
	G3HA23	Malate dehydrogenase (fragment)	0.09	9.49×10^{-3}
	G3HDQ2	Malate dehydrogenase	−0.18	1.90×10^{-2}
	G3HTR9	Malic enzyme (NAD)	−1.09	4.52×10^{-11}
Cholesterol biosynthesis	G3HMY0	3-Hydroxy-3-methylglutaryl coenzyme A synthase (HMG-CoA synthase)	−1.21	6.80×10^{-7}
	G3HP76	3-Hydroxy-3-methylglutaryl coenzyme A synthase (HMG-CoA synthase)	−0.86	9.79×10^{-7}
	G3GRT8	Diphosphomevalonate decarboxylase	−0.34	5.52×10^{-6}
	G3HC39	Farnesyl pyrophosphate synthetase	−0.70	2.35×10^{-8}
	G3H0L7	Squalene synthetase	−1.02	8.31×10^{-11}

Note: The logFC and the adjusted *p* value have been generated using limma empirical Bayes moderated *t* test. The BSO-treated condition ($n = 10$) have been compared to control conditions ($n = 12$).

Abbreviations: BSO, buthionine sulfoximine; CHO, Chinese hamster ovary; HMG-CoA, 3-hydroxy-3-methylglutaryl coenzyme A; LogFC, log fold change; TCA, tricarboxylic acid.

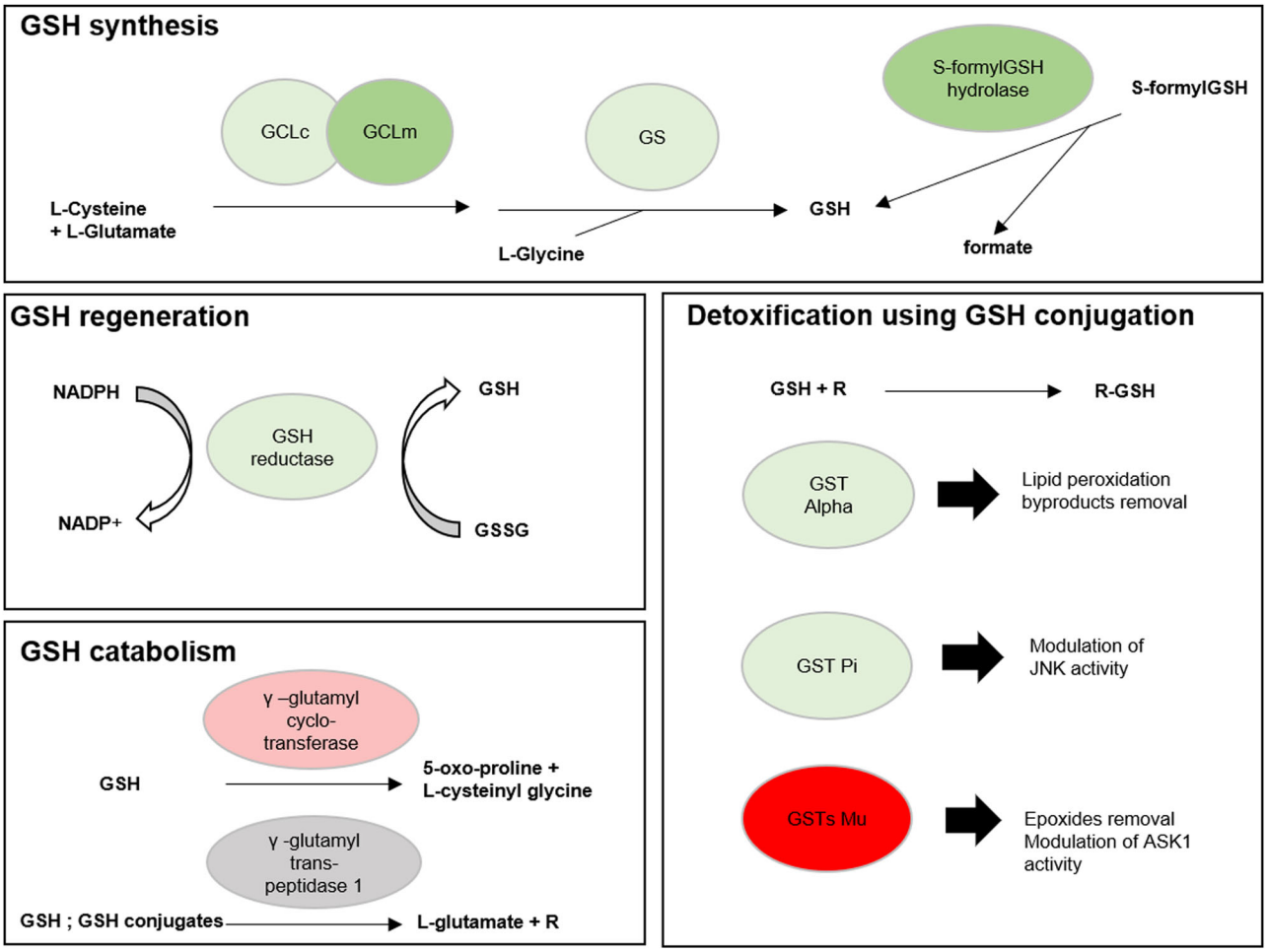

FIGURE 4 Glutathione metabolism-related proteins expression in BSO-treated cells. The logFC and the adj. *p* value are represented by the color from green to red. Red indicates a logFC > 0.5 and an adj. $p < .05$; light red indicates logFC < 0.5 and an adj. $p < .05$; green indicates a logFC < −0.5 and an adj. $p < .05$; light green indicates logFC > −0.5 and an adj. $p < .05$ and gray adj. $p > .05$. Statistical data have been generated using limma empirical Bayes moderated *t* test. The BSO-treated condition ($n = 10$) have been compared to control conditions ($n = 12$). BSO, buthionine sulfoximine; GCLc, glutamate–cysteine ligase; GCLm, glutamate–cysteine ligase modifier; GSH, glutathione; GSSG, glutathione disulfide; logFC, log fold change [Color figure can be viewed at wileyonlinelibrary.com]

from other families (omega, alpha, and pi) were not downregulated (Figure 4).

4 | DISCUSSION

In this study, to characterize oxidative stress response in CHO cells, we have modulated the GSH synthesis through two approaches: by the reduction of cysteine supply and by the inhibition of GSH biosynthesis. Reducing cysteine concentration in the feed by 50% did not appear to influence cell growth but led to a decrease of 24% in titer and of 50% in intracellular GSH. However, the inhibition of GCL activity by BSO led to significant depletion of GSH as well as a reduced cell growth and titer. In addition to classical physiological characterization and metabolite profiling, proteomics was performed at different stages of the culture. Interestingly, no significant differences in protein expression were observed in the reduced cysteine feed condition, whereas 63 proteins displayed different expression levels in the BSO-treated conditions suggesting an adaptation to oxidative stress.

In a recent study, it was shown that a decrease of cysteine supply led to a depletion of GSH (Ali et al., 2019). Therefore, the oxidative stress generated led to cell death, titer decrease, and differential expression of proteins. In our study, the decrease of cysteine supply did not lead to intracellular GSH depletion. Therefore, we did not observe cell death and significant protein differential expression (adj. $p < .05$, logFC threshold: 0.5), while specific productivity was substantially reduced. Indeed, a clear correlation over time between specific productivity and GSH intracellular concentration was observed. It can thus be suggested that in response to a reduced cysteine supply and therefore a reduced GSH availability, the cell metabolism initially decreases the recombinant protein production to reduce ROS production. The regulation of this phenomenon can be due to a differential expression of nondetected cellular proteins such

as transcription factors. It could also be due to other regulatory mechanisms such as protein phosphorylations, which are not detected in this type of proteomic analysis.

Partial inhibition of GCL using BSO has been suggested as a selection system to enrich for a cell population with higher productivity (Feary, Racher, Young, & Smales, 2017). In our case, specific productivity is not increased by BSO treatment. These differences can be related to the differences in plasmid maintenance in GS and DG44 cell lines. Indeed, in their study, the effect of BSO is observed on the GS cell line that utilizes selection on methionine sulfoximine, an analog of BSO, and an inhibitor of glutamine synthetase. However, the DG44 cell line used in this study utilizes a different selection system. However, the increase in cell diameter and the overexpression of GCLc and GCLm were consistent with previous observations (Feary et al., 2017). Interestingly, in the present study, GCLm was more overexpressed than GCLc in BSO-treated cells. In the control condition, GCLm expression decreases over time following the intracellular GSH increase. However, constitutive expression of GCLc was observed (Figure S6). Despite a likely higher level of GCLc protein in CHO cells, it looks as though the dynamic expression of GCLm is the most important parameter in the regulation of de novo synthesis of GSH during the process. In a previous study in CHO cells, it has been demonstrated that upregulation of GCLm by cell engineering increased GSH content, (Orellana et al., 2017). In the present study, in the presence of BSO, CHO cells try to compensate for GCL inhibition by producing more GCLm. However, this response was not able to restore normal intracellular GSH levels in our experimental conditions. As cystine cannot be used for GSH synthesis, it is possible that the potential secretion observed from Day 8 happened to avoid the accumulation of this amino acid in the cell. Indeed, cysteine/cystine accumulation can potentially influence the intracellular redox potential.

In addition to the attempt to upregulate GSH production when inhibited by BSO, cells recycled GSH through the overexpression of *S*-formylglutathione and GSH reductase. Likewise, GSH catabolism through the gamma-glutamyl cyclotransferase was downregulated. Interestingly, the GST Mu enzymes 1, 5, and 6 were downregulated. However, other GSTs from other families (omega, alpha, and pi) have been detected and were not interpreted as downregulated. This can be due to the difference of substrate selectivity. For example, GSTs Mu are in general more efficient for nucleophilic aromatic substitution and less selective than GSTs alpha (Eaton & Bammler, 1999; Salinas & Wong, 1999). GSTs alpha is the only family able to reduce hydroperoxides. They are also involved in lipid peroxidation by product detoxification such as acrolein and 4-hydroxy-2-nonenal (Stevens & Maier, 2008; Yang, Huycke, Herman, & Wang, 2016). Moreover, some GSTs can have additional activities to conjugation such as GST Pi 1 that can bind to c-Jun N-terminal kinase and GST Mu 1 that can bind to apoptosis signal-regulating kinase 1, and modulate apoptosis signaling pathways (Allocati, Masulli, Di Ilio, & Federici, 2018; Armstrong, 2010).

Beside GSH metabolism, other responses to oxidative stress were observed. The main one was the overexpression of the heme oxygenase 1 already observed on Day 6 and amplified on Day 10. Increase of the free heme detoxification is usually observed under oxidative stress (Gozzelino, Jeney, & Soares, 2010). However, we also observed an upregulation of the transferrin receptor protein 1 and the 5-aminolevulinate (ALA) synthase. The first is involved in iron transport and the second is the rate-limiting enzyme in heme synthesis. However, there is an inconsistency with the regulation of heme biosynthesis described in literature as ALA synthase is usually downregulated when the heme oxygenase 1 is upregulated (Ajioka, Phillips, & Kushner, 2006; Fujii et al., 2004).

The heme oxygenase 1 gene expression is regulated by the nuclear factor E2-related factor 2 (Nrf2). This factor is retained in the cytoplasm through a complex with Keap1 under normal conditions. Under oxidative stress, it is translocated to the nucleus and binds to the antioxidant response element. The overexpression of Gclm and heme oxygenase 1 in the BSO-treated cells suggests an activation of the Keap1–Nrf2 pathway. Moreover, sequestosome 1, also called p62, is also overexpressed (Supplementary Information Material). This protein is known to compete with Nrf2 for the interaction with Keap1 leading to a stabilization of free Nrf2 (Wei, Enaka, & Muragaki, 2019). Others proteins related to the antioxidant defense (catalase, superoxide dismutase [Mn], thioredoxin 1, GSH reductase) and nicotinamide adenine dinucleotide phosphate (NADPH) regeneration through the oxidative pentose phosphate pathway (glucose-6-phosphate 1-dehydrogenase, 6-phosphogluconate dehydrogenase) have been measured as differentially expressed in the BSO-treated cells, but with a lower logFC magnitude (Tonelli, Chio, & Tuveson, 2018; Table S1). This observation can support the hypothesis of Nrf2 activation. One of the limitations with this explanation is that GSTs Mu genes have also been described as Nrf2 target and are significantly downregulated.

Another response to oxidative stress is the downregulation of intracellular ROS production. The main source of ROS within the cell is the respiratory chain (Turrens, 2003). In this context, mitochondria proteins should be the main targets of activity reduction. The general downregulation of proteins involved in the oxidative phosphorylation and the TCA cycle observed in BSO conditions confirm this hypothesis. Acyl-CoA synthetase family member 2, involved in the activation of fatty acid is also downregulated (logFC = −0.79, adj. $p = 1.11 \times 10^{10}$). This observation suggested a decrease of acetyl CoA supply to the TCA through the beta-oxidation pathway. This hypothesis was supported by the downregulation of other enzymes involved in the beta-oxidation process such as the carnitine *O*-palmitoyltransferase 2 or the acetyl-CoA acetyltransferase (Table S1). Consequently, carbon fluxes through the TCA cycle were reduced and pyruvate accumulated in the cells. Indeed, glycolysis enzymes were not downregulated and the glucose uptake was constant. Other enzymes involved in pyruvate production such as the malic enzyme (NAD) were downregulated. Therefore, pyruvate surplus was converted to lactate and alanine which are produced from Day 6 in BSO-treated cells.

Another downregulated process in response to GSH depletion was lipid metabolism and especially the cholesterol de novo synthesis

pathway. Cholesterol plays a major role in membrane fluidity regulation. Moreover, cholesterol regulation may also play a role on protein secretion reduction as it is an essential building block of secretion vesicles (Wang, Thiele, & Huttner, 2000). Recently, it has been shown that the increase of cholesterol synthesis with the upregulation of a microRNA can increase the productivity of CHO cell lines by increasing their secretion capacity (Loh, Yang, & Lam, 2017). It is then possible that the increase of productivity and GSH content observed overtime during the process are also link to cholesterol regulation.

One hypothesis that can be proposed to explain the downregulation of cholesterol synthesis under GSH depletion is the accumulation of oxysterols in the ER. The expression of enzymes involved in cholesterol synthesis is regulated by a common transcription factor SREBP2. SERBPs are retained in the ER membrane by forming a complex with the SERBP cleavage-activating protein and the insulin-induced gene protein (Insig). The retention of the complex is controlled by cholesterol and by oxysterol concentrations (Howe et al., 2016). As oxysterol is a byproduct of cholesterol biosynthesis, it is a signal for cholesterol overproduction for the cell. Oxysterols can be enzymatically derived, especially by the cytochrome P450 reductase, or direct products of cholesterol autoxidation (Olkkonen, Béaslas, & Nissilä, 2012). Hence, it could be hypothesized that the BSO treatment led to an increase of oxysterols in the ER (Micheletta & Iuliano, 2006).

Another possible explanation is that the reduction of cholesterol synthesis could be an attempt to decrease the use of NADPH. Indeed, the 3-hydroxy-3-methylglutaryl coenzyme A (HMG-CoA) reductase uses two NADPH molecules to reduce HMG-CoA to mevalonate (Burg & Espenshade, 2011). Moreover, NADPH electrons are transferred by the cytochrome P450 reductase to squalene monooxygenase and lanosterol demethylase during cholesterol synthesis (Porter, 2015). In total, four NADPH molecules are used to produce one cholesterol molecule from acetyl-CoA, which is stoichiometrically a lot. Decreasing this activity may also help to maintain NADPH/$NADP^+$ redox homeostasis and indirectly counteract oxidative stress.

Another hypothesis is the downregulation of cholesterol to favorize GSH import in the mitochondria. Indeed, cholesterol has been reported as a mitochondrial GSH transport regulator (Ribas, García-Ruiz, & Fernández-Checa, 2016). Accumulation of cholesterol in the mitochondria membrane has been shown to impair the activity of some membrane proteins such as the 2-oxoglutarate carrier that exports 2-oxoglutarate in the cytosol in exchange of the import of GSH in the mitochondria. Moreover, it has been shown that the accumulation of mitochondrial cholesterol can damage the respiratory chain complexes assembly (Solsona-Vilarrasa et al., 2019). Under GSH depletion, the cells potentially tried to stabilize the mitochondria membrane and favorize GSH import in the mitochondria matrix by lowering cholesterol.

We showed that reducing GSH intracellular content by half led to a decreased productivity of heterologous protein production despite a modest number of changes in the cellular proteins' expression profile. However, GSH depletion resulted in an adaptation of GSH metabolism and triggered an oxidative stress response. In addition, cells died, and the recombinant protein was completely stopped. Thanks to these extreme conditions, this study have lighted up that the modulation GSH, thanks to BSO, also impacted lipid biosynthesis, especially cholesterol that plays a role in protein secretion. Thus, to finally figure out how GSH metabolism is linked to productivity, further work should include control of cholesterol metabolism.

ACKNOWLEDGMENTS

This study was supported by the Innovationsfonden (5189-00037B) and UCB Nordic A/S. The authors would like to thank Quentin Demeyere, Jonathan Stern, and Thomas Powell from UCB Pharma for their support and training on the analytical methods and software.

ORCID

Valentine Chevallier http://orcid.org/0000-0001-7596-4136
Erwin M. Schoof http://orcid.org/0000-0002-3117-7832
Mikael R. Andersen http://orcid.org/0000-0003-4794-6808
Christopher T. Workman http://orcid.org/0000-0002-2210-3743

REFERENCES

Ajioka, R. S., Phillips, J. D., & Kushner, J. P. (2006). Biosynthesis of heme in mammals. *Biochimica et Biophysica Acta*, *1763*(7), 723–736. https://doi.org/10.1016/j.bbamcr.2006.05.005

Ali, A. S., Raju, R., Kshirsagar, R., Ivanov, A. R., Gilbert, A., Zang, L., & Karger, B. L. (2019). Multi-omics study on the impact of cysteine feed level on cell viability and mAb production in a CHO bioprocess. *Biotechnology Journal*, *14*(4), 1800352. https://doi.org/10.1002/biot.201800352

Allocati, N., Masulli, M., Di Ilio, C., & Federici, L. (2018). Glutathione transferases: Substrates, inihibitors and pro-drugs in cancer and neurodegenerative diseases. *Oncogenesis*, *7*(1), 8. https://doi.org/10.1038/s41389-017-0025-3

Armstrong, R. N. (2010). Glutathione transferases, *Comprehensive toxicology* (4, 2nd ed., pp. 295–321). Oxford, UK: Elsevier.

Burg, J. S., & Espenshade, P. J. (2011). Regulation of HMG-CoA reductase in mammals and yeast. *Progress in Lipid Research*, *50*(4), 403–410. https://doi.org/10.1016/j.plipres.2011.07.002

Chakravarthi, S., & Bulleid, N. J. (2004). Glutathione is required to regulate the formation of native disulfide bonds within proteins entering the secretory pathway. *Journal of Biological Chemistry*, *279*(38), 39872–39879. https://doi.org/10.1074/jbc.M406912200

Chong, W. P., Thng, S. H., Hiu, A. P., Lee, D. Y., Chan, E. C., & Ho, Y. S. (2012). LC-MS-based metabolic characterization of high monoclonal antibody-producing Chinese hamster ovary cells. *Biotechnology and Bioengineering*, *109*(12), 3103–3111. https://doi.org/10.1002/bit.24580

Craig, R., Cortens, J. P., & Beavis, R. C. (2004). Open source system for analyzing, validating, and storing protein identification data. *Journal of Proteome Research*, *3*(6), 1234–1242. https://doi.org/10.1021/pr049882h

Dorfer, V., Pichler, P., Stranzl, T., Stadlmann, J., Taus, T., Winkler, S., & Mechtler, K. (2014). MS Amanda, a universal identification algorithm optimized for high accuracy tandem mass spectra. *Journal of Proteome Research*, *13*(8), 3679–3684. https://doi.org/10.1021/pr500202e

Eaton, D. L., & Bammler, T. K. (1999). Concise review of the glutathione S-transferases and their significance to toxicology. *Toxicological Sciences*, *49*(2), 156–164. https://doi.org/10.1093/toxsci/49.2.156

Feary, M., Racher, A. J., Young, R. J., & Smales, C. M. (2017). Methionine sulfoximine supplementation enhances productivity in GS-CHOK1SV

cell lines through glutathione biosynthesis. *Biotechnology Progress*, *33*(1), 17–25. https://doi.org/10.1002/btpr.2372

Fujii, H., Takahashi, T., Matsumi, M., Kaku, R., Shimizu, H., Yokoyama, M., … Morita, K. (2004). Increased heme oxygenase-1 and decreased delta-aminolevulinate synthase expression in the liver of patients with acute liver failure. *International Journal of Molecular Medicine*, *14*(6), 1001–1005.

Gozzelino, R., Jeney, V., & Soares, M. P. (2010). Mechanisms of cell protection by heme oxygenase-1. *Annual Review of Pharmacology and Toxicology*, *50*, 323–354.

Hedblom, A., Hejazi, S. M., Canesin, G., Choudhury, R., Hanafy, K. A., Csizmadia, E., … Wegiel, B. (2019). Heme detoxification by heme oxygenase-1 reinstates proliferative and immune balances upon genotoxic tissue injury. *Cell Death & Disease*, *10*(2), 72. https://doi.org/10.1038/s41419-019-1342-6

Howe, V., Sharpe, L. J., Alexopoulos, S. J., Kunze, S. V., Chua, N. K., Li, D., & Brown, A. J. (2016). Cholesterol homeostasis: How do cells sense sterol excess? *Chemistry and Physics of Lipids*, *199*, 170–178. https://doi.org/10.1016/j.chemphyslip.2016.02.011

Ketterer, B., Coles, B., & Meyer, D. J. (1983). The role of glutathione in detoxication. *Environmental Health Perspectives*, *49*, 59–69. https://doi.org/10.1289/ehp.834959

Kolde, R. (2015). *pheatmap: Pretty heatmaps [Software].*

Lau, L. F. (2011). CCN1/CYR61: The very model of a modern matricellular protein. *Cellular and Molecular Life Science*, *68*(19), 3149–3163. https://doi.org/10.1007/s00018-011-0778-3

Loh, W. P., Yang, Y., & Lam, K. P. (2017). miR-92a enhances recombinant protein productivity in CHO cells by increasing intracellular cholesterol levels. *Biotechnology Journal*, *12*(4), 1600488. https://doi.org/10.1002/biot.201600488

Micheletta, F., & Iuliano, L. (2006). Free radical attack on cholesterol: Oxysterols as markers of oxidative stress and as bioactive molecules. *Immunology, Endocrine & Metabolic Agents—Medicinal Chemistry*, *6*, 305–316. https://doi.org/10.2174/187152206777435618

Mulukutla, B. C., Mitchell, J., Geoffroy, P., Harrington, C., Krishnan, M., Kalomeris, T., … Hiller, G. W. (2019). Metabolic engineering of Chinese hamster ovary cells towards reduced biosynthesis and accumulation of novel growth inhibitors in fed-batch cultures. *Metabolic Engineering*, *54*, 54–68. https://doi.org/10.1016/j.ymben.2019.03.001

Olkkonen, V. M., Béaslas, O., & Nissilä, E. (2012). Oxysterols and their cellular effectors. *Biomolecules*, *2*(1), 76–103. https://doi.org/10.3390/biom2010076

Orellana, C. A., Marcellin, E., Gray, P. P., & Nielsen, L. K. (2017). Overexpression of the regulatory subunit of glutamate-cysteine ligase enhances monoclonal antibody production in CHO cells. *Biotechnology and Bioengineering*, *114*(8), 1825–1836. https://doi.org/10.1002/bit.26316

Orellana, C. A., Marcellin, E., Schulz, B. L., Nouwens, A. S., Gray, P. P., & Nielsen, L. K. (2015). High-antibody-producing Chinese hamster ovary cells up-regulate intracellular protein transport and glutathione synthesis. *Journal of Proteome Research*, *14*(2), 609–618. https://doi.org/10.1021/pr501027c

Phipson, B., Lee, S., Majewski, I. J., Alexander, W. S., & Smyth, G. K. (2016). Robust hyperparameter estimation protects against hypervariable genes and improves power to detect differential expression. *The Annals of Applied Statistics*, *10*(2), 946–963. https://doi.org/10.1214/16-AOAS920

Porter, T. D. (2015). Electron transfer pathways in cholesterol synthesis. *Lipids*, *50*(10), 927–936. https://doi.org/10.1007/s11745-015-4065-1

Rappsilber, J., Mann, M., & Ishihama, Y. (2007). Protocol for micro-purification, enrichment, pre-fractionation and storage of peptides for proteomics using StageTips. *Nature Protocols*, *2*(8), 1896–1906. https://doi.org/10.1038/nprot.2007.261

Ribas, V., García-Ruiz, C., & Fernández-Checa, J. C. (2014). Glutathione and mitochondria. *Frontiers in Pharmacology*, *5*, 151. https://doi.org/10.3389/fphar.2014.00151

Ribas, V., García-Ruiz, C., & Fernández-Checa, J. C. (2016). Mitochondria, cholesterol and cancer cell metabolism. *Clinical and Translational Medicine*, *5*(1), 22. https://doi.org/10.1186/s40169-016-0106-5

Ritchie, M. E., Phipson, B., Wu, D., Hu, Y., Law, C. W., Shi, W., & Smyth, G. K. (2015). limma powers differential expression analyses for RNA-sequencing and microarray studies. *Nucleic Acids Research*, *43*(7), e47. https://doi.org/10.1093/nar/gkv007

Salinas, A. E., & Wong, M. G. (1999). Glutathione S-transferases—A review. *Current Medicinal Chemistry*, *6*(4), 279–309.

Solsona-Vilarrasa, E., Fucho, R., Torres, S., Nunez, S., Nuno-Lambarri, N., Enrich, C., … Fernandez-Checa, J. C. (2019). Cholesterol enrichment in liver mitochondria impairs oxidative phosphorylation and disrupts the assembly of respiratory supercomplexes. *Redox Biology*, *24*, 101214. https://doi.org/10.1016/j.redox.2019.101214

Sonnhammer, E. L., & Ostlund, G. (2015). InParanoid 8: Orthology analysis between 273 proteomes, mostly eukaryotic. *Nucleic Acids Research*, *43*(Database issue), D234–D239. https://doi.org/10.1093/nar/gku1203

Stevens, J. F., & Maier, C. S. (2008). Acrolein: Sources, metabolism, and biomolecular interactions relevant to human health and disease. *Molecular Nutrition & Food Research*, *52*(1), 7–25. https://doi.org/10.1002/mnfr.200700412

Tonelli, C., Chio, I. I. C., & Tuveson, D. A. (2018). Transcriptional regulation by Nrf2. *Antioxidants & Redox Signaling*, *29*(17), 1727–1745. https://doi.org/10.1089/ars.2017.7342

Turrens, J. F. (2003). Mitochondrial formation of reactive oxygen species. *Journal of Physiology*, *552*(Pt 2), 335–344. https://doi.org/10.1113/jphysiol.2003.049478

UniProt Consortium (2018). UniProt: A worldwide hub of protein knowledge. *Nucleic Acids Research*, *47*(D1), D506–D515. https://doi.org/10.1093/nar/gky1049

Wang, Y., Thiele, C., & Huttner, W. B. (2000). Cholesterol is required for the formation of regulated and constitutive secretory vesicles from the trans-Golgi network. *Traffic*, *1*(12), 952–962.

Wei, R., Enaka, M., & Muragaki, Y. (2019). Activation of KEAP1/NRF2/P62 signaling alleviates high phosphate-induced calcification of vascular smooth muscle cells by suppressing reactive oxygen species production. *Scientific Reports*, *9*(1), 10366. https://doi.org/10.1038/s41598-019-46824-2

Yang, Y., Huycke, M. M., Herman, T. S., & Wang, X. (2016). Glutathione S-transferase alpha 4 induction by activator protein 1 in colorectal cancer. *Oncogene*, *35*(44), 5795–5806. https://doi.org/10.1038/onc.2016.113

SUPPORTING INFORMATION

Additional supporting information may be found online in the Supporting Information section.

How to cite this article: Chevallier V, Schoof EM, Malphettes L, Andersen MR, Workman CT. Characterization of glutathione proteome in CHO cells and its relationship with productivity and cholesterol synthesis. *Biotechnology and Bioengineering*. 2020;117:3448–3458. https://doi.org/10.1002/bit.27495